

What binds quarks together at different momentum scales? A conceptual scenario

N. G. Stefanis*

*Institut für Theoretische Physik II,
Ruhr-Universität Bochum, D-44780 Bochum, Germany*

(Dated: October 8, 2014)

The binding effects of quarks within hadrons are discussed in terms of the pion distribution amplitude over longitudinal momentum fractions. To understand the behavior of this quantity at different momentum scales, the concept of synchronization in complex systems has been employed. It is argued that at low momentum scales, the quarks get correlated by nonlocal quark/gluon condensates that cause an endpoint-suppressed, mainly bimodal structure of the pion distribution amplitude inferred from a sum-rule analysis. The mass generation mechanism, within the framework of Dyson-Schwinger equations, and evolution effects pull these two peaks back to the center to form at $Q^2 \rightarrow \infty$ the asymptotic distribution amplitude which represents the most synchronized $\bar{q}q$ state.

PACS numbers: 12.38.Aw, 05.45.Xt, 11.10.Hi, 14.40.Be

1. Introduction. One of the greatest unsolved problems in Quantum Chromodynamics (QCD) is the confinement phenomenon responsible for the binding effects of partons—quarks and gluons—within hadrons (see [1, 2] for recent reviews). While at large momenta and energies, the color forces in the parton interactions can be adequately and systematically described by perturbative QCD, the regime of large distances, alias, small momenta, cannot be treated reliably in perturbation theory. The key for the success of perturbative QCD in the ultraviolet domain is grounded in the fact that the strong coupling becomes weaker as the distances between interacting partons decrease, giving ultimately rise to an asymptotically free field theory—“ultraviolet freedom” [3].

On the other hand, the behavior of the strong coupling constant in the infrared (IR) has not yet been formally established. However, various calculations, based on the Dyson-Schwinger equations (DSE), yield clear signs for the saturation of color forces in the IR, see, e.g., [4] for a recent review. Standard QCD perturbation theory cannot be reliably applied at low Euclidean momenta because of the inevitable appearance of the (unphysical) Landau singularity at momenta $\mu^2 \sim \Lambda_{\text{QCD}}^2$. Several proposals exist to rectify this problem and define an analytic coupling in the IR—see [5] for a review. Nevertheless, it is still unclear how the confining properties of quarks and gluons, encoded in correlation functions, arise in nonperturbative QCD. Certainly, lattice calculations can provide useful benchmarks for the confinement phase of QCD, but they have their own inherent limitations. In search of alternatives, and without the mathematical tools to solve QCD nonperturbatively in the continuum, we need new ideas and organizing principles to guide us through the data in hopes of revealing tangible predictions that can be used to test these concepts.

In this paper, I will describe a “roadmap” to confinement by synthesizing different new and old ideas and methods to form a unified perception of this phenomenon without formally solving the QCD correlation functions in a deep mathematical sense. Nevertheless, predictions will be presented that can be tested in experiments in the near future. A novelty of the approach is the use of the concept of spontaneous synchronization of nonlinear oscillators, that has passed the test of experiment in various areas of nonlinear science, but has never been used before in the context of QCD.

To begin with, What are the landmarks along the confinement route? Instead of starting at high momenta and march down to small ones, where confinement becomes eminent for quarks, I will describe a scenario that goes the inverse way and discuss the behavior of interlocked quarks from low to large momentum scales. I will expose this scenario in three steps: (i) nonperturbative correlations, (ii) dynamical chiral-symmetry breaking (DCSB) and mass generation, and (iii) evolution behavior from low to (asymptotically) high momenta. The following exposition will be basic but precise.

2. Nonperturbative correlations. What binds quarks together? Although we cannot answer this question by performing ab initio calculations within continuum QCD, we may try to understand the salient features of what binds quarks together at *different* momentum scales by pursuing multiple approaches and combining their results. The primary concern in analyzing a hadronic process within QCD is how to describe as much as possible of its dynamics in terms of hard (i.e., short-distance) partonic subprocesses—characterized by a large scale Q^2 —amenable to QCD perturbation theory. The large-distance (soft) remainder—ascribed to nonperturbative dynamics—is then taken from experiment. This factorization procedure becomes particularly useful, if the isolated soft part is universal, i.e., process independent. Using techniques from collinear factorization, a good “laboratory” for testing these issues is provided by the process-independent pion’s distribution amplitude (DA)

*Electronic address: stefanis@tp2.ruhr-uni-bochum.de

$\varphi_\pi(x, \mu^2)$ for finding the valence $\bar{q}q$ pair in the pion carrying the longitudinal momentum fractions $x_q = x$ and $x_{\bar{q}} = 1 - x \equiv \bar{x}$. On the other hand, the large momentum scale Q^2 localizes the hard collisions of the partons in the longitudinal direction along the lightcone (see [6–8] for reviews).

The pion DA is the prototype for a two-body bound state in QCD and is defined at the leading-twist level two by the matrix element

$$\langle 0 | \bar{q}(z) \gamma_\mu \gamma_5 [z, 0] q(0) | \pi(P) \rangle |_{z^2=0} = i f_\pi P_\mu \int_0^1 dx e^{ix(z \cdot P)} \times \varphi_\pi^{(2)}(x, \mu^2). \quad (1)$$

It is linked to the lightcone wave function of the $\bar{q}q$ pair [7]: $\varphi_\pi^{(2)}(x, \mu^2) = \int^{\mu^2} \frac{d\mathbf{k}_T^2}{16\pi^2} \psi(x, \mathbf{k}_T)$. The momentum scale μ enters through the renormalization of the current operator and denotes the maximum transverse momentum included in the lightcone wave function of the $\bar{q}q$ pair. We have adopted in (1) the lightcone gauge $A \cdot n = 0$, where $n^2 = 0$, so that the gauge link $[z, 0] = \mathcal{P} \exp(i g \int_0^z A^\mu d\tau_\mu) = 1$. We have also used the shorthand notation $A^\mu = \sum_a t^a A_a^\mu$ (t_a being the generators of $SU(3)_c$), whereas the symbol \mathcal{P} path-orders these matrix-valued quantities along the lightlike vector n from 0 to z . The dependence of the pion DA on the scale μ is controlled by the Efremov-Radyushkin-Brodsky-Lepage (ERBL) evolution equation [9, 10]. Though the pion DA is not directly observable, it can be used within a factorization-based approach to calculate form factors that can be measured in experiments.

Historically, one assumes a non-trivial vacuum that is populated by quark $\langle 0 | \bar{q}q | 0 \rangle$ and gluon $\langle 0 | G^{\mu\nu} G_{\mu\nu} | 0 \rangle$ field condensates with a correlation length much larger than the typical hadronic size [11]. Focusing on the quark condensate, with the fields taken at the same point (therefore, local), this is equivalent to say that the average virtuality is zero, corresponding to an infinite correlation length of the vacuum fluctuation. This concept of “local” vacuum condensates has been used for decades in QCD sum rules and has provided valuable insight into the structure of hadrons, see [6] for a review. However, the description of dynamical quantities, such as quark distribution amplitudes for hadrons, faces severe problems (see, e.g., [12]) that are entailed by the local character (zero-quark virtuality) of the quark condensate. Moreover, an infinite correlation length of the quark condensate would lead to a cosmological constant several orders of magnitude larger than observation [13].

The use of nonlocal condensates in QCD sum rules (NLC-SR)s was proposed by Radyushkin and collaborators quite long ago [14–16]. More recently, this approach was updated and refined by Bakulev, Mikhailov, Stefanis (BMS) in [17] with the goal to extract the twist-two pion DA at the scale $\mu^2 \approx 1 \text{ GeV}^2$ in terms of the expansion coefficients, $a_2, a_4, a_6, a_8, a_{10}$ within the complete orthonormal basis on $x \in [0, 1]$ of the Gegenbauer poly-

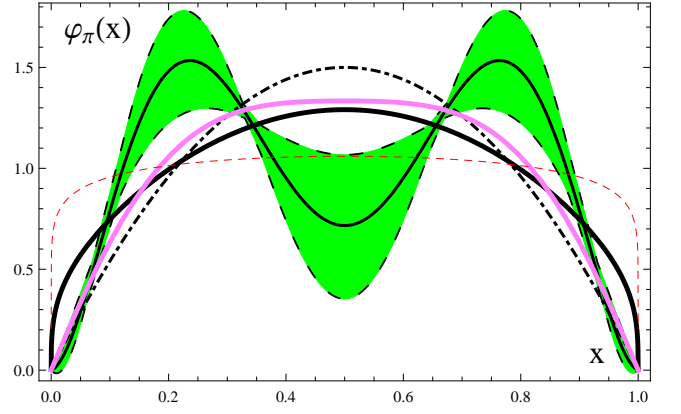


Figure 1: (color online) Shaded (green) band contains the two-parametric BMS DAs at $\mu^2 \approx 1 \text{ GeV}^2$ [17]. Curves: dashed, flat-top DA at $\mu^2 = 1 \text{ GeV}^2$ from [20]; lower solid, DSE-based approach [21] at $\mu^2 = 4 \text{ GeV}^2$; dashed-dotted, asymptotic DA. Upper thick (pink) solid line shows the shorttailed platykurtic DA [22] at $\mu^2 = 4 \text{ GeV}^2$.

nomials $C_n^{3/2}(2x - 1)$ (isospin symmetry applied):

$$\varphi_\pi^{(2)}(x, \mu^2) = \varphi_\pi^{\text{asy}}(x) + \sum_{n=2,4,\dots}^{\infty} a_n(\mu^2) \psi_n(x), \quad (2)$$

where $\varphi_\pi(x, \mu^2 \rightarrow \infty) = \varphi_\pi^{\text{asy}}(x) = 6x\bar{x}$ is the asymptotic pion DA and $\psi_n(x) = 6x\bar{x} C_n^{3/2}(2x - 1)$. Inverting the moments $\langle \xi^N \rangle = \int_0^1 dx (2x - 1)^N \varphi_\pi^{(2)}(x, \mu^2)$, with the normalization condition $\int_0^1 dx \varphi_\pi^{(2)}(x, \mu^2) = 1$, it was found [17] $a_2^{\text{BMS}}(1 \text{ GeV}^2) = (7/12)(5\langle \xi^2 \rangle - 1) \approx 0.20$, $a_4^{\text{BMS}}(1 \text{ GeV}^2) = (77/8)(\langle \xi^4 \rangle - (2/3)\langle \xi^2 \rangle + (1/21)) \approx -0.14$, while the coefficients a_6, a_8, a_{10} were also determined but were neglected in the modeling because they were found to be significantly smaller than the first two and bearing large uncertainties, see [17, 18] for details. This DA is shown in Fig. 1 as a solid line inside the shaded (green) band which contains the whole family of two-parametric pion DAs enclosed by the envelopes $[a_2 = 0.134, a_4 = -0.044]$ and $[a_2 = 0.251, a_4 = -0.207]$ (from top to bottom). This two-parametric DA family complies with the moment values determined from the QCD NLC-SR with nonlocal condensates at $\mu^2 \approx 1 \text{ GeV}^2$ considered in [17] and yields values for the inverse moment $\langle x^{-1} \rangle_\pi = \int_0^1 \varphi_\pi(x) x^{-1} dx = 3(1 + a_2 + a_4 + a_6 + \dots)$ which comply within errors with those determined via an independent sum rule [17], $\langle x^{-1} \rangle_\pi^{\text{BMS}} = 3.35 \pm 0.3$. This implies that the sum of all coefficients a_n is dominated by the contribution of a_2 and a_4 , a result which lends credibility to the BMS DA family. Moreover, the value $a_2 = 0.19 \pm 0.06$ conforms with the recent lattice estimates of the RBC and UKQCD Collaborations [19].

As one observes from Fig. 1, one key characteristic of this type of DAs (shaded band in green color) is that the regions at the kinematic endpoints $x \approx 0$ and $x \approx 1$ are strongly suppressed — even relative

to the asymptotic DA (dashed-dotted line) [20]. This suppression is entailed by the finiteness of the average quark virtuality $\lambda_q^2 = \langle \bar{q}(0)D^2q(0) \rangle / \langle \bar{q}(0)q(0) \rangle \simeq \langle \bar{q}igG^{\mu\nu}\sigma_{\mu\nu}q \rangle / 2\langle \bar{q}(0)q(0) \rangle \approx [0.35 - 0.5] \text{ GeV}^2$, where $D_\mu = \partial_\mu - ig\Sigma_a A_\mu^a t^a$ and $G^{\mu\nu}$ is the gluon-field strength tensor. In the following, the value $\lambda_q^2(\mu^2 \approx 1 \text{ GeV}^2) \approx 0.4 \text{ GeV}^2$ will be used, which was determined in [17] with the help of the CLEO data [23] on the pion-photon transition form factor—see [24] for lattice estimates and references. The parameter λ_q^2 controls the strength of the nonlocal condensate contribution in the QCD sum rules: the larger its value, the stronger suppressed this contribution and the closer the shape of the pion DA becomes to the asymptotic form. Technically speaking, the profile of the BMS DAs results from the interplay between the perturbative contribution and the dominant nonperturbative term due to the scalar nonlocal condensate in the theoretical part of the QCD sum rule. Because the latter contribution is not singular in x and has a dip around $x = 1/2$, it causes a bimodal endpoint-suppressed structure of the DA profile.

The crucial assumption underlying the nonlocality of the condensate is that in coordinate space the correlation length $\Lambda \sim 1/\lambda_q$ for a $\bar{q}q$ pair behaves like $\langle \bar{q}(z)[z, 0]q(0) \rangle \sim \langle \bar{q}(0)q(0) \rangle \exp(-\lambda_q^2|z|^2/8)$. Such a distribution function of Gaussian fluctuations means that the $\bar{q}q$ correlation length induced by the condensate tends to stay within a limited range, which is about $\Lambda \sim 0.3 \text{ fm}$ (for $\lambda_q^2 = 0.4 \text{ GeV}^2$ [17]). At large Euclidean z^2 , the nonlocal quark condensate decays rapidly to zero [20, 24], so that, from a distance, the virtuality fluctuations are ironed out and the condensate practically exists only inside hadrons (similarly to the in-hadron condensates proposed in [13, 25]). If we calculate the average transverse momentum of a valence quark in the pion with the help of the $\bar{q}q$ pair wave function $\psi(x, \mathbf{k}_T)$, assuming again a Gaussian distribution for the intrinsic \mathbf{k}_T momenta carried by the quarks [26], we find $\langle \mathbf{k}_T^2 \rangle_{\text{BMS}}^{1/2} \sim 0.35 \text{ GeV}$ which amounts to a distance of approximately $0.6 \text{ fm} \approx \langle r_\pi^2 \rangle^{1/2}$ (the pion’s charge radius). This value is about the same for the values $m_q = 0$ and $m_q \approx 0.3 \text{ GeV}$, we used, and agrees well with the estimate in [6]. On the other hand, gluons decouple and disperse their transverse momentum to an infinite number of gluons via their self-interactions. Thus, the vacuum field fluctuations are much shorter than the typical transverse size of the valence-quark state—see [26] for details. These findings are in line with the appearance of DCSB on a scale $\sim 0.3 \text{ fm}$, see, e.g., [27].

3. Synchronization concepts. The most obvious characteristic of the BMS pion DA is its two-humped structure, which is condensate-driven and reflects the tension between the valence quark and the valence antiquark with respect to their longitudinal momentum fractions. To comprehend the meaning of the pion DA at different momentum scales, it is helpful to conceive of the longitudinal momentum fractions x as being nat-

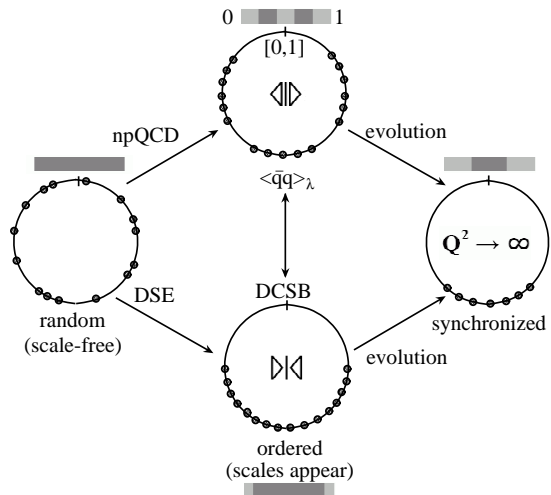


Figure 2: (color online). Pion DAs at different momentum scales in terms of the Kuramoto model. The dots represent x values in the interval $[0, 1]$. The tension ($\langle \Diamond \rangle_\lambda$) and compression ($\langle \blacktriangleright \blacktriangleleft \rangle_\lambda$) tendencies in the x spectrum are indicated. The strips show the dominant x regions in the corresponding DAs.

ural oscillator frequencies (phases) of a large number ($N \rightarrow \infty$) of phase-coupled oscillators using the Kuramoto model—see [28] for reviews and references.¹ As long as the oscillators are non-interacting, their native frequencies—visualized in an idealized way as a swarm of points randomly distributed on a unit circle of $x \in [0, 1]$ —are unlocked building an incoherent ensemble of points (left portrait in Fig. 2). This situation corresponds to a constant pion DA, or a flat-top one that vanishes at the kinematical endpoints $x = 0, 1$, e.g., $\varphi_\pi^{\text{flat-top}}(x) = \Gamma(2(\alpha + 1))[\Gamma^2(\alpha + 1)]^{-1}(x\bar{x})^\alpha$ with $\alpha = 0.1$ —dashed (red) line in Fig. 1 [20].² Such a distribution is scale-free, meaning that no x region is singled out to be associated with a valence quark (antiquark) because all locations on the unit circle are indistinguishable; the pion looks like a pointlike particle without internal structure, see, for example, [29]. Besides, $\varphi_\pi(x) = \text{const}$ (corresponding to a vanishing pion charge radius) would yield results for the electromagnetic and transition form factors in conflict with experiment [29].

The nonlocal condensate $\langle \bar{q}q \rangle_\lambda$, as a clear manifestation of nonperturbative QCD, creates a color-singlet proto-pion and causes the set of the x values in the pion DA to flock into two distinct clusters: one close to $x \approx 0.75$, the other at $x \approx 0.25$. These clusters correspond to two groups of synchronized oscillators (upper graph in Fig. 2), whereas the endpoints $x = 0, 1$ around the “North pole” are almost depleted. This pattern con-

¹ The technical details of this model are not relevant for our qualitative exposition.

² A “table-like” pion DA $\varphi_\pi^{\text{table}}(x) \simeq (x\bar{x})^{0.05}/0.91$ with $\lambda_q^2 \sim 0.35 \text{ GeV}^2$ was proposed in [15].

forms with the generic profile of a BMS-like DA in Fig. 1. It suggests that most configurations of the valence $\bar{q}q$ pair tend to have either a leading quark or a leading antiquark, though configurations in which the valence quark and the valence antiquark share comparable fractions of the longitudinal momentum of the pion around $x = 1/2$ are also possible but are less favorable. In accordance with Fig. 1, the size of the two clusters bears large uncertainties.³ The same applies to the region around the “South pole” in Fig. 2, which corresponds to the central region $x = 1/2$ in Fig. 1, while the absence of dots around the “North pole” is quite strict. This is, because in our approach [17] the uncertainties on the shape of the π DA in the endpoint regions $x = 0, 1$ are very small (see Fig. 1).

Note that the well-known Chernyak-Zhitnitsky DA [6] would correspond to a pattern (not shown) with two distinct clusters concentrated at the endpoints $x = 0, 1$, while the central region $x = 1/2$ would be almost empty.

4. DCSB and mass generation. The other important feature of confinement is DCSB and the generation of quark and gluon masses. At a deeper level of understanding of the QCD dynamics in the IR, it is likely that condensate formation and mass generation are intertwined phenomena. However, at present it is prudent to discuss these effects separately using specific schemes. An appropriate framework to study the mass-generation effects is provided by the DSE-based method, see [30] for a recent review. The dressed-quark mass ~ 0.3 GeV converts the real quark pole in the dressed quark propagator into a complex one, whereas the *effective* gluon mass, with a dressed-gluon mass scale in the range 0.4–0.6 GeV [30], enters the argument of the strong coupling and provides saturation of the color forces in the IR. In Fig. 1 we show a pion DA—solid (blue) line—obtained with the DSE methodology [21, 30–32]—Eq. (15) in [21]. It derives from the nonperturbative content of the Bethe-Salpeter kernels in the dressed quark and gluon propagators associated with DCSB, the later being exclusively responsible for the broadening of this DA relative to φ_π^{asy} [21]. At the renormalization point $\mu = 2$ GeV it is described by the concave function $\varphi_\pi^{\text{DSE}}(x) = 1.81(x\bar{x})^a[1 + \tilde{a}_2 C_2^{a+1/2}(2x - 1)]$ with $a = 0.31$, $\tilde{a}_2 = -0.12$. A similarly downward concave DA, $\varphi_\pi^{\text{AdS/QCD}}(x) = (8/\pi)(x\bar{x})^{1/2}$, was derived within a holographic approach to QCD embedded in a five-dimensional Anti-de Sitter (AdS) space [33]. Using the Kuramoto model, the portrait of φ_π^{DSE} is represented by the graph at the bottom in Fig. 2. It describes a pack of partially synchronized oscillators with natural frequencies in a wide range of x values. Similar considerations apply to the AdS/QCD DA.

Thus, the “true” pion DA seems to be determined

by the balance of two competing effects: the correlation caused by the $\langle \bar{q}q \rangle_\lambda$ condensate, pushing the x values away from the center at $x = 1/2$ to form a two-cluster arrangement, and DCSB which tends to enhance the central x region by broadening the shape of the DA and create—speaking in terms of the Kuramoto-model analogy—a single moderately synchronized group of oscillators (see Fig. 2). One might argue that at low scales, $\mu \approx 2$ GeV, $\varphi_\pi^{\text{true}}(x) \approx a\varphi_\pi^{\text{BMS}}(x) + (1 - a)\varphi_\pi^{\text{DSE}}(x)$.⁴ This synthesized DA would have features pertaining to both confinement facets, exhibiting profile characteristics inherited from both DAs: endpoint suppression like φ_π^{BMS} and central-region enhancement like φ_π^{DSE} . For $a \approx 0.7 - 0.9$, it would still belong to the family of BMS-like DAs shown in Fig. 1 within the shaded area yielding an inverse moment $[\langle x^{-1} \rangle_\pi = 3(1 + a_2 + a_4 \dots) = 3/(\sqrt{2}f_\pi)Q^2 F_{\gamma^* \gamma \pi^0}^{(\text{LO})}(Q^2)]$ with values in the range $\langle x^{-1} \rangle_\pi^{\text{true}} \sim \langle x^{-1} \rangle_\pi^{\text{BMS}} \lesssim 3.5 < \langle x^{-1} \rangle_\pi^{\text{DSE}} \approx 4.6$ and, as a result, a pion-photon transition form factor (TFF) inside the margin of predictions in Fig. 3. The accurate determination of the mixing parameter a , which controls the tradeoff between the endpoint suppression and the broadness of the π DA, will be discussed separately in a future publication. Here suffice it to say that one may select within the BMS scheme a DA which is a downward concave curve over a broad interval of x values but which still exhibits endpoint suppression entailed by the nonlocal condensate [22]. This short-tailed platykurtic pion DA belongs to a family of admissible DAs derived with the nonlocality $\lambda_q^2 = 0.45$ GeV² and is displayed in Fig. 1 (thick solid pink line). The close resemblance between this DA and the DSE one is obvious. But the distinct behavior from the DSE DA at the endpoints is key in deriving predictions for the pion-photon TFF in good agreement with the data (see Fig. 3). As the pion DA evolves to higher Q^2 , QCD interactions die out and the DA reaches at $Q^2 \rightarrow \infty$ its asymptotic form which represents the most synchronized $\bar{q}q$ configuration (Fig. 2).

5. Litmus test of the approach. The scenario exposed above, can be tested experimentally by measuring the pion-photon TFF $F^{\gamma^* \gamma \pi^0}(q_1^2 = Q^2, q_2^2 \rightarrow 0)$ with $Q^2 \gg \Lambda_{\text{QCD}}^2$. This is the gold-plated QCD observable because it arises from the factorization properties of QCD, with all binding nonperturbative effects being absorbed into the twist-two and twist-four pion DAs. Hence, the Q^2 behavior of this TFF reflects and reveals the underlying structure of the pion DA. The calculation of $F^{\gamma^* \gamma \pi^0}$ has been carried out within our approach—based on lightcone sum rules (LCSR)s [34–36]—in [37] and subsequently in [38], with technical details being provided in [18]. The TFF within the method of LCSRs is calculated with the help of Eq. (2) in [18] using the expressions pro-

³ Inclusion of more coefficients a_n would eventually entail more and smaller clusters.

⁴ This would imply that at nonperturbative scales ψ^{true} is a superposition of ψ^{BMS} and ψ^{DSE} (or AdS/QCD).

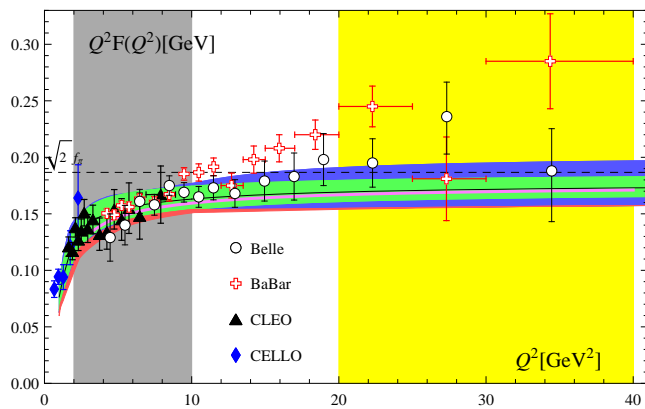


Figure 3: (color online) Scaled pion-photon TFF vs. Q^2 in comparison with data. The designations are given in the text.

vided in App. A and App. B in the same reference. The upshot of this calculation are state-of-the-art predictions, shown in Fig. 3. The broad horizontal (green) band represents the TFF which uses as input the two-parametric family of BMS DAs, discussed above, and includes the NLO perturbative corrections, i.e., T_{LO} and T_{NLO} , as well as the twist-four term in terms of an effective twist-four DA [35], while the main next-to-next-to-leading order contribution, T_{NNLO} , is taken into account together with the twist-six term [39] in the form of uncertainties (see [18] for details). ERBL evolution is also included at NLO. The narrower (blue) strips above and below the broader (green) one show the influence of the uncertainties induced by the next higher coefficient a_6 , while the very narrow (red) strip, at lower Q^2 values, represents the effect on the calculated TFF of a non-vanishing virtuality of the quasireal photon caused by the untagged electron in the Belle experiment [40] with the value $q_2^2 \approx 0.04 \text{ GeV}^2$, as detailed in [18]. The pink line just below the BMS one (central line of the band) denotes the prediction obtained with the platykurtic DA and has

similar statistical accuracy with respect to the data. The presented predictions for the endpoint-suppressed DAs of our approach agree very well with all existing data that are compatible with QCD scaling: CELLO [41], CLEO [23], and Belle [40]. The same applies to the BaBar data [42] below 9 GeV^2 . However, there is no matching between our scaling predictions and the auxetic behavior of the high Q^2 BaBar data above 10 GeV^2 [18].

There are two momentum regimes for the pion-photon TFF which will be probed experimentally by two different collaborations in the near future—see Fig. 3. Window I (shaded area towards the left): Measurement data with high statistics in the spacelike region $2 < Q^2 < 10 \text{ GeV}^2$, taken with the BESIII (Beijing Spectrometer) detector at the BEPC-II (Beijing Electron Positron Collider) facility, in $e^+e^- \rightarrow \pi^+\pi^- J/\Psi$ collisions can be used to study TFFs of light mesons [43]. Window II (shaded area towards the right): Single-tagged measurements of the pion TFF will be performed with the Belle II detector at the upgraded KEKB accelerator (SuperKEKB) in Japan in the next few years and are expected to cover a wide range of momenta up to about 50 GeV^2 , where the data is much sparser. A confirmation of the predictions in Fig. 3 will provide a key piece of evidence for the presented approach.

6. Conclusions. In conclusion, I have aggregated different concepts and methods together in order to provide insight into the inner structure of the $\bar{q}q$ component of the pion DA as it appears at different momentum scales from the typical hadronic domain to the asymptotic regime. While the binding effects at low momenta are mainly due to nonlocal condensates, combined with mass dressing owing to DCSB, at very high momentum the quarks in the pion are in lockstep only as a result of synchronization.

Acknowledgments. I would like to thank Sergey Mikhailov and Alexander Pimikov for collaboration and discussions.

-
- [1] N. Brambilla, et al., arXiv:1404.3723 [hep-ph].
 - [2] K. I. Kondo, S. Kato, A. Shibata and T. Shinohara, arXiv:1409.1599 [hep-th].
 - [3] D. J. Gross and F. Wilczek, Phys. Rev. Lett. 30 (1973) 1343; H. D. Politzer, Phys. Rev. Lett. 30 (1973) 1346.
 - [4] P. Boucaud, et al., Few Body Syst. 53 (2012) 387.
 - [5] N. G. Stefanis, Phys. Part. Nucl. 44 (2013) 494.
 - [6] V. Chernyak and A. Zhitnitsky, Phys. Rept. 112 (1984) 173.
 - [7] S. J. Brodsky and G. P. Lepage, High Energy Phys. 5 (1989) 93.
 - [8] N. G. Stefanis, Eur. Phys. J. direct C 7 (1999) 1.
 - [9] A. Efremov and A. Radyushkin, Theor. Math. Phys. 42 (1980) 97; Phys. Lett. B 94 (1980) 245.
 - [10] G. P. Lepage and S. J. Brodsky, Phys. Rev. D 22 (1980) 2157.
 - [11] M. A. Shifman, A. I. Vainshtein, and V. I. Zakharov, Nucl. Phys. B 147 (1979) 385; B 147 (1979) 448; B 147 (1979) 519.
 - [12] A. V. Radyushkin, Nucl. Phys. A 527 (1991) 153C-164c.
 - [13] S. J. Brodsky, C. D. Roberts, R. Shrock, and P. C. Tandy, Phys. Rev. C 82 (2010) 022201.
 - [14] S. V. Mikhailov and A. V. Radyushkin, JETP Lett. 43 (1986) 712; Sov. J. Nucl. Phys. 49 (1989) 494; A. P. Bakulev and A. V. Radyushkin, Phys. Lett. B 271 (1991) 223; S. V. Mikhailov, Phys. Atom. Nucl. 56 (1993) 650.
 - [15] S. V. Mikhailov and A. V. Radyushkin, Sov. J. Nucl. Phys. 52 (1990) 697.
 - [16] S. V. Mikhailov and A. V. Radyushkin, Phys. Rev. D 45 (1992) 1754.
 - [17] A. P. Bakulev, S. V. Mikhailov, and N. G. Stefanis, Phys. Lett. B 508 (2001) 279; B 590 (2004) 309(E).
 - [18] N. G. Stefanis, A. P. Bakulev, S. V. Mikhailov, and A. V. Pimikov, Phys. Rev. D 87 (2013) 094025.

- [19] R. Arthur, et al., Phys. Rev. D 83 074505 (2011).
- [20] S. V. Mikhailov, A. V. Pimikov, and N. G. Stefanis, Phys. Rev. D 82 (2010) 054020.
- [21] L. Chang et al., Phys. Rev. Lett. 110 (2013) 132001.
- [22] S. V. Mikhailov, A. V. Pimikov, and N. G. Stefanis, work in progress.
- [23] J. Gronberg et al. (CLEO), Phys. Rev. D 57 (1998) 33.
- [24] A. P. Bakulev and S. V. Mikhailov, Phys. Rev. D 65 (2002) 114511.
- [25] S. J. Brodsky, C. D. Roberts, R. Shrock, and P. C. Tandy, Phys. Rev. C 85 (2012) 065202.
- [26] N. G. Stefanis, W. Schroers, and H.-C. Kim, Phys. Lett. B 449 (1999) 299; Eur. Phys. J. C 18 (2000) 137.
- [27] P. Schweitzer, EPJ Web Conf. 66 (2014) 06022.
- [28] S. H. Strogatz, Physica D 143 (2000) 1; J. A. Acebron, et al., Rev. Mod. Phys. 77 (2005) 137.
- [29] L. Chang, C. D. Roberts, and P. C. Tandy, Chin. J. Phys. 49 (2011) 955.
- [30] I. C. Cloet and C. D. Roberts (2013), Prog. Part. Nucl. Phys. 77 (2014) 1.
- [31] P. Maris and C. D. Roberts, Phys. Rev. C 56 (1997) 3369; C 58 (1998) 3659.
- [32] F. Gao et al., arXiv:1405.0289 [nucl-th].
- [33] S. J. Brodsky and G. F. de Teramond, Phys. Rev. D 77 (2008) 056007; S. J. Brodsky, F.-G. Cao and G. F. de Teramond, Phys. Rev. D 84 (2011) 033001; D 84 (2011) 075012; S.J. Brodsky, G. F. de Teramond and H. G. Dosch, Few Body Syst. 55 (2014) 407.
- [34] I. I. Balitsky, V. M. Braun, and A. Kolesnichenko, Nucl. Phys. B 312 (1989) 509.
- [35] A. Khodjamirian, Eur. Phys. J. C 6 (1999) 477.
- [36] A. Schmedding and O. Yakovlev, Phys. Rev. D 62 (2000) 116002.
- [37] A. P. Bakulev, S. V. Mikhailov, and N. G. Stefanis, Phys. Rev. D 67 (2003) 074012; Phys. Lett. B 578 (2004) 91.
- [38] A. P. Bakulev, S. V. Mikhailov, and N. G. Stefanis, Phys. Rev. D 73 (2006) 056002; S. V. Mikhailov and N. G. Stefanis, Nucl. Phys. B 821 (2009) 291; A. P. Bakulev, S. V. Mikhailov, A. V. Pimikov, and N. G. Stefanis, Phys. Rev. D 84 (2011) 034014; D 86 (2012) 031501(R).
- [39] S. S. Agaev, V. M. Braun, N. Offen, and F. A. Porkert, Phys. Rev. D 83 (2011) 054020; D 86 (2012) 077504.
- [40] S. Uehara et al. (Belle Collaboration), Phys. Rev. D 86 (2012) 092007.
- [41] H. J. Behrend et al. (CELLO), Z. Phys. C 49 (1991) 401.
- [42] B. Aubert et al. (The BaBar), Phys. Rev. D 80 (2009) 052002.
- [43] M. Unverzagt, J. Phys. Conf. Ser. 349 (2012) 012015.